## SPECIAL ISSUE - RESEARCH ARTICLE





# MALDI imaging directed laser ablation tissue microsampling for data independent acquisition proteomics

#### Correspondence

Dr Kermit K. Murray, 331 Choppin Hall, Department of Chemistry, Louisiana State University, LA 70803, United States. Email: kkmurray@lsu.edu

#### Funding information

National Science Foundation, Grant/Award Number: CHE-1709526

### Abstract

A multimodal workflow for mass spectrometry imaging was developed that combines MALDI imaging with protein identification and quantification by liquid chromatography tandem mass spectrometry (LC-MS/MS). Thin tissue sections were analyzed by MALDI imaging, and the regions of interest (ROI) were identified using a smoothing and edge detection procedure. A midinfrared laser at 3-µm wavelength was used to remove the ROI from the brain tissue section after MALDI mass spectrometry imaging (MALDI MSI). The captured material was processed using a single-pot solid-phase-enhanced sample preparation (SP3) method and analyzed by LC-MS/MS using ion mobility (IM) enhanced data independent acquisition (DIA) to identify and quantify proteins; more than 600 proteins were identified. Using a modified database that included isoform and the post-translational modifications chain, loss of the initial methionine, and acetylation, 14 MALDI MSI peaks were identified. Comparison of the Kyoto Encyclopedia of Genes and Genomes (KEGG) pathways of the identified proteins was achieved through an evolutionary relationships classification system.

## 1 | INTRODUCTION

Matrix-assisted laser desorption/ionization mass spectrometry imaging (MALDI MSI) is a powerful tool to visualize the spatial distribution of a wide range of biomolecules in tissue sections. <sup>1-6</sup> MALDI MSI has been used as a complementary tool to histology, and applications include biomarker discovery, disease classification, tumor heterogeneity determination, <sup>4,9</sup> and monitoring the distribution of drugs and metabolites in tissue to assess different stages of drug discovery and development. One of the major challenges of MALDI MSI for compound identification is the presence of many tissue components that can lead to ion suppression and obscure the analyte signal from low abundant molecules. Additionally, the presence of potential protein isoforms that result from alternative splicing and post-translational modification (PTM)<sup>12,13</sup> make protein identifications in unseparated mixtures challenging.

Liquid chromatography coupled with mass spectrometry (LC-MS) can aid in identifying and quantifying a large number of biomolecules from tissue extracts; however, in most cases, LC-MS analyses do not preserve tissue or sample localization information. A number of recent approaches to coupling MALDI MSI and LC-MS in a single workflow have demonstrated the potential to extend the capabilities of mass spectrometry imaging. <sup>24,78,14</sup> These studies have shown that MALDI MSI can be used to locate ROI and LC-MS/MS can be employed to identify and quantify the associated biomolecules. <sup>15</sup>

Successful coupling of MALDI MSI and LC-MS requires efficient extraction of small quantities of material from tissue. For example, direct liquid extraction can be used to sample biomolecules from selected regions of tissue sections. With the direct liquid extraction method, a volume of an appropriate solvent is automatically or manually deposited on the section to extract biomolecules, and the extracted material is removed and analyzed using LC-MS/MS. Sampled areas can range from a fraction of a millimeter to several millimeters in diameter. This workflow has been used for assignment of MALDI MSI peaks 17,19,20 and to characterize ROI defined by MSI. 21,22

Localized sampling can also be achieved by manual microdissection, where a small portion of the tissue section is removed using

<sup>&</sup>lt;sup>1</sup>Department of Chemistry, Louisiana State University, Baton Rouge, LA 70803, United States

<sup>&</sup>lt;sup>2</sup>Department of Chemistry and Biochemistry, Baylor University, Waco, TX 76706, United States

a pipette or needle under a microscope.<sup>23,24</sup> The use of a thin polymer layer such as parafilm between the tissue and microscope slide prevents direct contact of tissue with the glass surface and facilitates the microdissection.<sup>25,26</sup> Parafilm assisted microdissection (PAM) has been used for metabolite identification and quantification parallel to a proteomics workflow for identification of multiple biochemical pathways.<sup>27</sup>

An alternative to manual microdissection is laser capture microdissection (LCM), which uses an ultraviolet (UV) or infrared (IR) laser to remove ROI from a tissue section. Two general methods are used: UV-cutting and IR melting. With UV cutting, the ROI boundary is irradiated by the focused laser and then detached with pulses of the unfocused laser at the center of the ROI. Resolution IR melting employs an IR laser to melt a thermoplastic film that covers the tissue section and is removed together with the ROI. LCM has been coupled with LC-MS/MS and MALDI MSI. Sa-38

Laser ablation and capture can be used to remove material from tissue sections by converting it to small particles that are ejected from the tissue into a capture vial or analysis system. Laser ablation uses a pulsed UV,  $^{39,40}$  visible,  $^{41}$  or IR  $^{42-49}$  laser to irradiate the regions of tissue section in transmission (back side irradiation) or reflection (front-side radiation) geometry.  $^{43}$  The mid-IR wavelength of 2.94  $\mu m$  overlaps with OH vibrational absorption of water as well as molecules containing a hydroxyl group and is efficient at biomolecule ablation without fragmentation.  $^{51,52}$  Mid-IR laser ablation has been used for ablation capture and offline analysis of proteins,  $^{50}$  peptides,  $^{43}$  enzyme,  $^{53}$  DNA,  $^{54}$  and RNA  $^{55}$  while preserving their molecular integrity.

In the work described here, MALDI MSI was coupled with laser ablation sampling for offline protein identification and quantification using UPLC-HDMS<sup>E</sup> (ie, IM enhanced DIA). Contours generated from MALDI MSI were used to define ROI, and the same tissue section was used for laser ablation sampling. Bottom up protein identification and label-free quantification were achieved using UPLC-HDMS-E. The list of identified proteins was used for identification of MALDI MSI peaks.

## 2 | EXPERIMENTAL

## 2.1 | Sample preparation

Fresh rat brain tissue samples (Pel-Freez Biologicals, Rogers, AR) were sectioned at -20°C using a cryostat (CM 1850, Leica Microsystem, Wetzlar, Germany). Optimal cutting temperature solution (OCT, Sakura Finetek, Torrance, CA) was used to fix one side of the organ to the cryostat support, avoiding contact of the OCT solution with the exposed side of the organ. Coronal tissue sections at 10-µm thickness were thaw-mounted on indium tin oxide (ITO) coated microscope slides (University Wafer, South Boston, MA) at -25°C. Sections were stored at -80°C prior to further sample processing.

Prior to MALDI MSI, tissue sections were vacuum dried for 10 minutes and washed with 70% ethanol for 45 seconds and 95%

ethanol for 45 seconds to remove lipids and salts. After washing the tissue sections were vacuum dried for another 10 minutes before matrix application. Sinapic acid (SA, Sigma-Aldrich, St. Louis, MO) matrix was prepared at a concentration of 10 mg/mL in ~70:30 methanol:water with 0.1% TFA. The matrix was applied to the tissue section by spraying with a pneumatic nebulizer comprising a 200- $\mu$ L micropipette tip, a quarter-inch stainless steel compression fitting tee (Swageloc, Solon, OH), and a silica capillary with a 75  $\mu$ m I.D. and 360  $\mu$ m O.D. The nebulizer was connected to a compressed air source operating at 10 psig pressure. A 3-mL syringe and syringe pump (NE-300, Pump Systems Inc., Farmingdale, NY) were used to deliver the matrix solution at a flow rate of 100  $\mu$ L/min.

#### 2.2 | MALDI MSI

MALDI MSI experiments were performed using a MALDI-TOF/TOF mass spectrometer (UltrafleXtreme, Bruker Daltonics, Billerica, MA) operated in positive-ion reflectron mode. The MALDI matrix was sprayed on the tissue section using a pneumatic nebulizer. Mass spectra were acquired at a range of 2000 to 30 000 m/z. The target raster was 150 μm with 1000 shots per pixel, and the random walk option was set to 25 shots per position. After MALDI MSI, tissue sections were stored at -80°C until laser ablation sampling.

The MALDI images of selected m/z values were normalized to the total ion current (TIC) and created using FlexImaging software. The MALDI images were processed with Adobe Photoshop. The Gaussian Blur and Trace Contour functions were applied utilizing the mean ( $\mu$ ) and standard deviation ( $\sigma$ ) of the image histograms, and the resulting images were used to determine the ROI. Protein quantification for MALDI MSI was accomplished using ImageJ (version 1.52a, National Institutes of Health, Bethesda, MD). ImageJ was used to overlay the ROI on the MALDI image and retrace their contour for a particular protein. The ImageJ Measure tool was used to sum pixel intensities within the ROI on the MALDI image corresponding to that protein, and the pixel intensity was normalized to the ROI area for protein quantification.

## 2.3 | Laser ablation

Laser ablation was performed on tissue sections after MALDI MSI. It was found that more proteins were identified when the matrix was removed after imaging (Supplementary Material Figure S1). Matrix removal was accomplished by washing tissue sections with 70% ethanol for 1 minutes for 10 minutes. The mid-IR laser ablation system has been previously described. Briefly, a tunable wavelength ( $\lambda$  = 2940 nm) pulsed (20 Hz) nanosecond (7-ns temporal width) IR optical parametric oscillator (IR Opolette; OPOTEK, Carlsbad, CA, USA) was used to irradiate samples using a transmission geometry. The laser beam was directed at the target at a 45° angle and focused with a 50-mm focal length lens. The laser spot size was 200  $\mu$ m × 250  $\mu$ m determined by burn paper at 2-mJ laser energy. The laser energy was adjusted with an

external dual-plate attenuator. Microscope slides were mounted on a two-dimensional translation stage (Model-433; Newport, Irvine, CA, USA) which was operated using 50-mm motorized actuators (LTA-HS, Newport). A CMOS camera (DCC1645C, Thor Laboratories, Newton, NJ) was used for viewing samples. A LabVIEW program was used to translate the slide in two dimensions for ablating the selected area at a velocity of 1 mm/s. The stages were moved in a line raster pattern with a line spacing of 100  $\mu$ m. The ablated material was captured in a 300- $\mu$ L microcentrifuge tube (mounted 5 mm below the ablation spot) containing 200  $\mu$ L of 50 mM tris buffer (pH = 8.5) with 1% sodium dodecyl sulfate (SDS, Sigma-Aldrich).

## 2.4 | Protein digestion

Single-pot solid-phase-enhanced sample preparation (SP3) was used for tissue digestion and filter aided sample preparation (FASP).50 Further details can be found in Supplementary Material Figure S2. SP3 digestion was achieved using carboxylate modified magnetic particles (Speed Beads or Sera-Mag, GE Life Sciences, Chicago, IL, USA).58 The magnetic beads were added at a ratio of 1:1 (v/v), washed with water three times, and reconstituted in water at a concentration of 20 μg/μL Protein disulfide bond reduction was achieved by adding DLdithiothreitiol (DTT, Sigma-Aldrich) to each sample tube to a final DTT concentration of 10 mM followed by incubation at 100°C for 45 minutes, then the samples were kept at room temperature for 15 minutes. Alkylation was performed by adding iodoacetamide (Sigma-Aldrich) to each sample to a final concentration of 20 mM followed by incubation in the dark for 30 minutes. After reduction and alkylation, 2 µL of the bead solution was added into each reaction. After the addition of bead solution, ACN was added to each 300-µL Eppendorf tube to obtain a final concentration of 60% (v/v). These samples were incubated at room temperature for 20 minutes followed by incubation on a magnetic rack for 2 to 5 minutes until the beads settled on the magnets. Protein clean-up was achieved by adding 70% ethanol, incubating for 5 minutes off the magnetic rack, and then incubating on the magnetic rack for another 2 minutes. This procedure was repeated twice with 70% ethanol and once with ACN before drying at 37°C. The samples were re-suspended in 10-µL ammonium bicarbonate buffer and sonicated for 5 minutes prior to trypsin digestion.

Trypsin (Promega, Madison, WI) digestion was performed with an enzyme to protein ratio of 1:20 (v/v). Samples were incubated at 37°C overnight and shaken at 300 rpm with a thermal mixer (Thermo Scientific, Waltham, MD, USA). The washing steps (twice with 70% ethanol, once with 100% ACN) were repeated followed by recovering the peptides by adding 10- $\mu$ L 0.1% formic acid (in DI H<sub>2</sub>O) and sonication for 5 minutes. The samples were then incubated on the magnetic rack for 2 to 5 minutes, and the supematant was collected, avoiding aspiration of any beads. Tryptic peptide mixtures obtained from SP3 were vacuum dried and stored at  $-20^{\circ}$ C until analysis.

# 2.5 | HDMS<sup>E</sup> analysis

Rat brain digests were analyzed with a Synapt G2-S HDMS system and nanoACQUITY UPLC system (Waters, Milford, MA, USA). Mobile phase Solvent A was water, and Solvent B was ACN (each with 0.1% FA). The peptides were desalted on a Symmetry C18 pre-column (5 μm, 20 mm × 180 μm) and separated on a BEH130 C18 analytical reversed-phase column (1.7 μm, 100 mm × 100 μm) at a column temperature of 40°C. For each sample, a 5.0-µL partial loop injection was transferred to the precolumn for desalting and preconcentration using 99% Solvent A at a flow rate of 10 mL/min for 3 minutes. The preconcentrated peptides were eluted to the analytical column and separated for 90 minutes using a gradient of 5% to 45% Solvent B at a flow rate of 600 nL/min. Following the separation, the mobile phase was ramped to 99% Solvent B for 5 minutes and held at 99% Solvent B for an additional 5 minutes. The mobile phase was ramped to 5% Solvent B over 5 minutes, and the column was re-equilibrated at 5% Solvent B for 15 minutes. During the runs, the lock mass compound, [Glu1]-fibrinopeptide B (Waters) at a concentration of 300 fmol/mL was delivered to the reference sprayer at 500 nL/min.

MS was performed in positive-ion electrospray ionization mode (ESI), and the time-of-flight (TOF) mass analyzer of the Synapt G2-S HDMS was operated in sensitivity mode (V mode) with 10 000 FWHM resolution. The TOF was externally calibrated from m/z 50 to 2000 using a sodium formate solution, and all TOF data were lock-mass corrected postacquisition using the doubly charged monoisotopic ion of the lock compound, [Glu1]-fibrinopeptide B at m/z 785.8426. UPLC data independent acquisition was performed using the ion mobility (IM)-enhanced "MSE Continuum" function of MassLynx, HDMS<sup>E</sup> employs IM separation in conjunction with TOF detection, using alternating low (4 V) and high (15 to 45-V ramp) collision energies for collecting parallel data of precursor and product ions. During the UPLC-HDMS<sup>E</sup> experiments, the IM cell was filled with ~3.5 mbar nitrogen gas. Acquisition times for low and high energy scans were 1 second each. Additional details of the IM settings are provided in Supplementary Material Table S1.

ProteinLynx Global Server (PLGS Ver. 2.5.2; Waters Corporation) was used for peptide identification with the following parameters: UniprotKB/Swiss-Prot rattus norvegicus proteome database; two missed cleavages; 5 ppm precursor and fragment ion mass tolerances; ≥3 ion matches per peptide; carbamidomethyl C fixed modification; oxidation M variable modification; false positive rate of 5. Identified peptides with at least five amino acid lengths were used for BLAST analysis using in-house software (Protein and Imaging Tools (PIT), ver. 1.0.2, https://github.com/FabrizioDonnarumma/PIT.git) and UniprotKB/Swiss-Prot rattus norvegicus proteome database (Uniprot 2018\_3). The database was modified using PIT to include single protein entry with chain, initiator methionine, signal peptide, and transit peptide post translational modifications. Proteins with at least two matched peptides were considered identified.

Functional annotation was performed using the Database for Annotation, Visualization, and Integrated Discovery bioinformatics resource (DAVID 6.8).<sup>59,60</sup> The Kyoto Encyclopedia of Genes and Genomes (KEGG) database was used for pathway analysis and KEGG pathways with at least five proteins and P value <0.05 were considered. Proteins in the same pathway were output into the Search Tool for Recurring Instances of Neighboring Genes (STRING 10.5) to generate protein-protein interaction networks.<sup>61</sup> Both physical and functional associations are considered for protein-protein interactions in STRING; only the interactions among identified proteins were considered. The minimum required interaction score was set at 0.4 (medium confidence).<sup>62,63</sup> Label-free protein quantification of UPLC-HDMS<sup>E</sup> results was performed by summing the signal from the three most abundant unique peptides.

## 3 | RESULTS AND DISCUSSION

MALDI images were obtained from sections from a single rat brain. Two of the sections were consecutive, mounted on the same ITO slide, and imaged sequentially. The third section was not consecutive and was mounted on a separate ITO slide. Approximately 30 peaks were observed in the average MALDI mass spectra in the m/z range from 3000 to 30 000 m/z.

Figure 1 shows 14 MALDI images that can be sorted into three general types: homogeneous signal throughout (Figure 1A,B,I), signal most intense in the corpus callosum and hippocampus (Figure 1C-F, K,N), and signal least intense in the corpus callosum and hippocampus (Figure 1G,H,J,L,M). For example, (blue) images generated from 8569, 14 041, and 17 139 m/z had relatively homogeneous intensities that were similar in all areas of the constructed images. Conversely, (green) images generated from 14 122, 14 132, 14 192, 14 211, 18 401, and 28 217 m/z had intense signals in the corpus callosum and hippocampus regions whereas (magenta) images at 15 193, 15 845, 17 737, 21 912, and 22 092 m/z had relatively low signals in the corpus callosum and hippocampus regions.

Figure 2 shows MALDI MSI ROI contours generated from the images in Figure 1 using Gaussian smoothing. Heat map images

generated by mass spectrometer software were saved as 8-bit Tagged Image File Format (TIFF) files and loaded into Adobe Photoshop. The images were smoothed using the Gaussian Blur function with a radius of 10, which corresponds to a standard deviation of 2.1 mm in the MALDI images. This radius was found to be efficient for generating relatively smooth and contiguous regions from the MALDI images obtained in this study. Region of interest contour lines were generated using the Photoshop Trace Contour function using the mean (µ) and standard deviation (o) values from the smoothed image intensity level histogram that indicates the number of pixels with a specific intensity value in the range from 0 to 255. Three contour lines were obtained: lower quintile ( $\mu$  - 1.28 $\sigma$ ), mean ( $\mu$ ), and upper quintile ( $\mu$  + 1.28 $\sigma$ ). The homogeneous (blue) images at 8569, 14 041, and 17 139 m/z have corresponding homogeneous ROI that largely span the entire brain. The intense corpus callosum/hippocampus images (green) have corresponding ROI centered on those regions, whereas the weak signal corpus callosum/hippocampus images (magenta) have ROI largely excluding those regions. The corpus callosum and hippocampus ROI were used to guide laser ablation sampling.

For all three tissue sections, the ROI were selected using the 14 122 m/z (Figures 2C and 3A) image which corresponds to myelin basic protein (MPB) isoform 4 (Uniprot: PO2688). 56,64,65 The upper quintile (light green, Figure 3A) was used as a guide for ROI selection. Figure 3B shows an optical microscope image of a tissue section after laser ablation. Three contiguous areas were ablated and captured from each tissue section at a laser fluence of 20 kJ/m². Two of those areas that encompassed a 7 mm² total area of the corpus callosum and hippocampus regions were collected in one microcentrifuge tube as ROI 1. The third region that covered a 4-mm² midbrain region was collected in a separate microcentrifuge tube as ROI 2. Brain regions were identified using a rat brain atlas and correspond to Rat P21 Figure 51. 66 The ROI 1 and ROI 2 samples were digested using the SP3 method and analyzed using UPLC-HDMS<sup>E</sup>.

Figure 4 shows representative MS and MS/MS spectra from ROI 1.

Product ions were correlated with their corresponding precursor ion

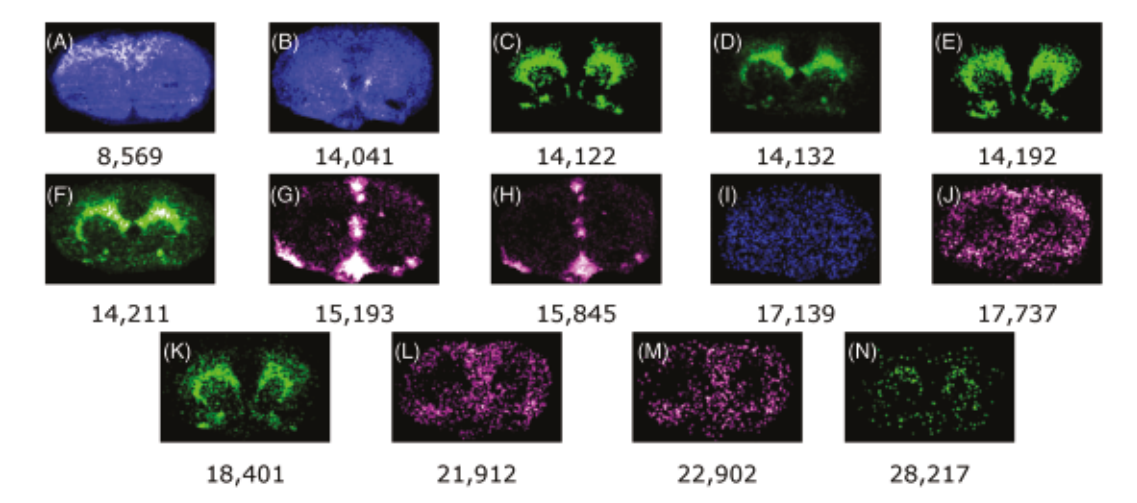


FIGURE 1 Representative MALDI images of rat brain tissue sections obtained using peaks at (A) 8569, (B) 14 041, (C) 14 122, (D) 14 132, (E) 14 192, (F) 14 211, (G) 15 193, (H) 15 845, (I) 17 139, (J) 17 737, (K) 18 401, (L) 21 912, (M) 22 902, and (N) 28 217 m/z

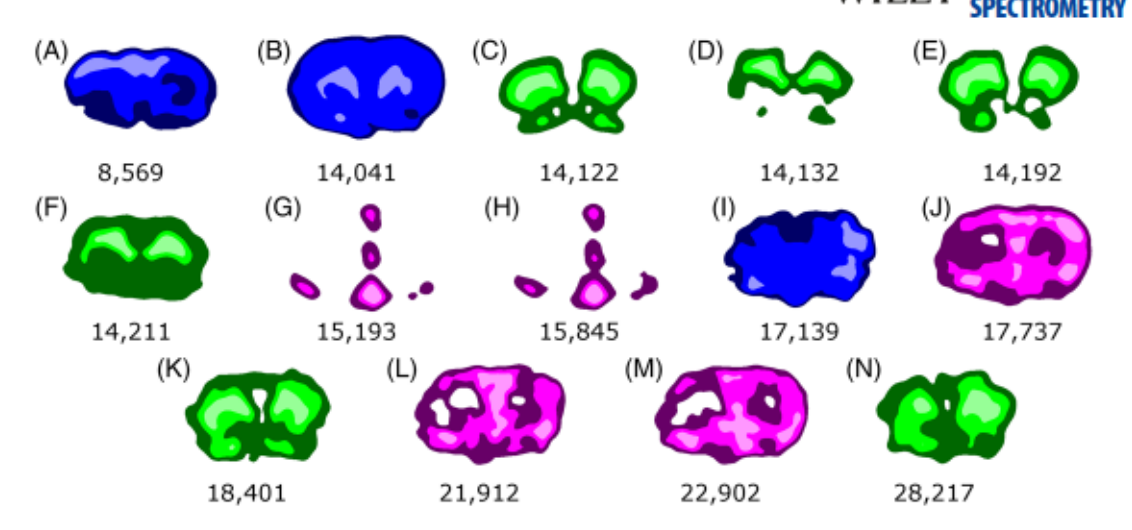
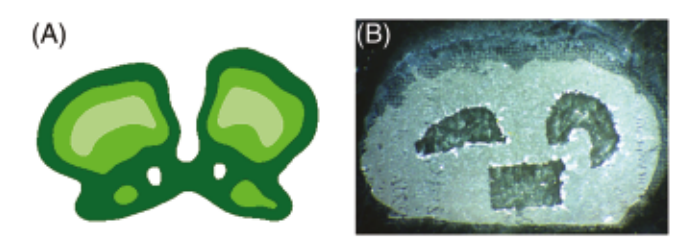


FIGURE 2 Contour maps obtained from MALDI MSI from peaks at (A) 8569, (B) 14 041, (C) 14 122, (D) 14 132, (E) 14 192, (F) 14 211, (G) 15 193, (H) 15 845, (I) 17 139, (J) 17 737, (K) 18 401, (L) 21 912, (M) 22 902, and (N) 28 217 m/z; the color shade indicates signal intensity with the light shade indicating the upper quintile (>80%), midcolor intensity indicates mean (50%-80%), and dark indicates the lower quintile (20%-50%)



**FIGURE 3** (A) Contour of MALDI MSI at 14 122 m/z; (B) bright-field microscope image of laser ablated rat brain tissue. Location 1, corpus callosum and hippocampus (7 mm<sup>2</sup>); Location 2, midbrain (4-mm<sup>2</sup> square)

with PLGS using the LC retention time and IM drift time. Figure 4B shows a tandem MS spectrum that corresponds to the triply charged precursor ion at 446 m/z (Figure 4A), [M + 3H]<sup>3+</sup>. A series of immonium ions and consecutive singly/doubly charged y-series ions from y<sub>5</sub> to y<sub>11</sub> were observed. The peptide was identified as YLATASTMDHAR which is unique to the myelin basic protein family (all MBP isoforms).

Peptides and proteins identified in ROI 1 and ROI 2 in three replicate tissue sections are summarized in Table S2. An average of 398 ± 129 proteins were identified from three tissue sections in the 7-mm² ROI 1, and an average of 268 ± 43 proteins were identified in the 4-mm² ROI 2. A total of 3024 peptides were identified, about 7% of which were found in all samples. A total of 636 proteins from three rat brain tissue sections were identified, a third of which were found in all six samples. The discrepancy in total protein number between Sections a and b and Section c may result from the fact that Section c is not immediately consecutive to the other two sections, and it is possible that differences between these sections are not clearly evident by visual inspection. However, it should be noted that the sample cohort size in this work is not sufficiently large to evaluate sampling

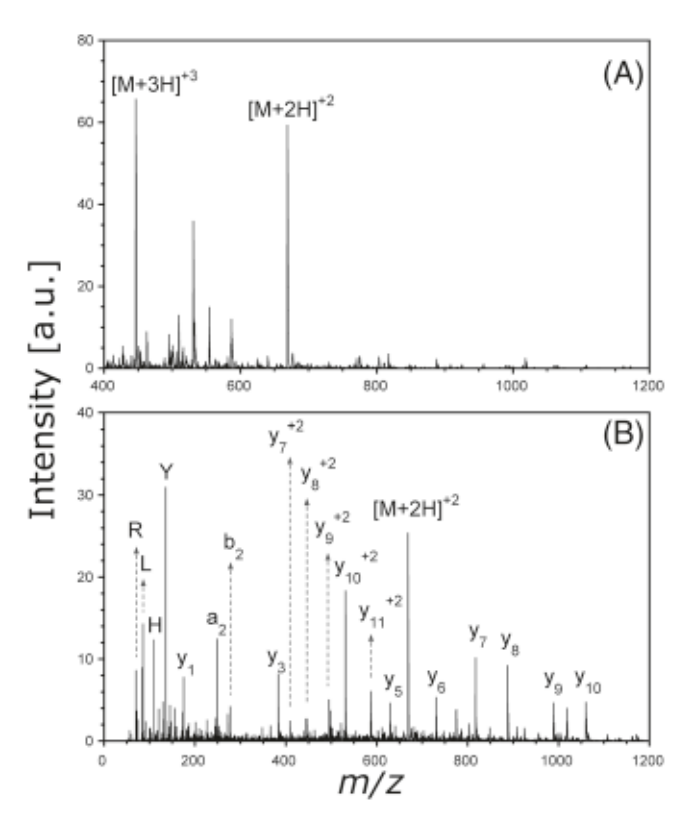


FIGURE 4 Representative UPLC-HDMSE data from analysis of tissue: (A) MS spectrum for myelin basic protein (MBP) unique peptide "YLATASTMDHAR"; (B) MS/MS spectrum for "YLATASTMDHAR"

and biological variability, both of which play a role in determining the total number of proteins identified. Unique peptides and proteins were also identified in each of the six samples. About 45% of the identified peptides and 31% of the identified proteins were found in only one of the six samples. Some peptides and proteins were common to multiple sampling sections and positions. For example, hemoglobin, actins, and tubulins were found in all six regions of the three sections, most likely because they are highly expressed and relatively ubiquitous in tissue. The number of proteins identified was comparable to that reported in a previous study.<sup>67</sup>

The masses of the proteins identified by UPLC-HDMS<sup>E</sup> were used for MALDI MSI peak identification. The MALDI MSI peak m/z values were searched against the list of UPLC-HDMS<sup>E</sup> identified protein masses assuming singly charged protonated molecules. A peak was considered a potential match if the m/z value for the peak was within 500 ppm of the protonated species. This value was chosen because the MALDI system calibration prior to MALDI MSI was conducted with this tolerance. In addition to protein mass, the following sequence modifications were considered as potential MALDI MSI matches: (a) protein chain (polypeptide resulting from enzymatic cleavage of the original protein), (b) isoform (a structurally similar protein with one or more different amino acids), (c) loss of the initial methionine, and (d) acylation. These four protein modifications were used because of their common occurrence. Other common PTMs such as phosphorylation or glycosylation were not considered in this initial proof-of-concept study for the sake of simplicity. Potential assignments of the MALDI MSI peaks based on UPLC-HDMS<sup>E</sup> identified

protein masses and the above modification are summarized in the Table 1. Fourteen MALDI MSI peaks were identified. The identified peaks include cell junction protein, cytoskeletal protein, chaperone, and nucleic acid binding proteins.

Laser ablation sampling and UPLC-HDMS<sup>E</sup> allowed precise relative quantification of the MBP protein family (all the MBP isoforms) in the selected region. MBP quantification using MALDI MSI was achieved by summing the intensity of the 14 122 m/z signal (MBP-4) from each pixel within each ROI. The fraction of MBP-4 in ROI 2 was 13 ± 4% of that observed in ROI 1. The peptides identified in the UPLC-HDMS<sup>E</sup> data were common to all isoforms of MBP, and there was no unique peptide for MBP-4 that was not common to the other isoforms. In a previous study, an antibody was developed to stain MBP isoforms that were extracted from specific brain regions such as the cerebellum. These isoforms were further fractionated to separate them in individual samples for gel electrophoresis.<sup>68</sup> The results indicate that all isoforms are observed in the tested regions, but with different signal intensity. A similar result was obtained using liquid microextraction of protein material from rat brain tissue. Although the entire brain was not analyzed, gel electrophoresis of material extracted from the corpus callosum displayed all isoforms of MPB at differing concentrations. 69 Therefore, to account for the multiple isoforms, MBP quantification using UPLC-HDMS<sup>E</sup> was performed by summing the three

**TABLE 1** Summary of all MALDI peaks assigned based on LC-MS/MS analysis of the laser ablated extracts including the molecular weight (MW) of the identified proteins, molecular weight difference (ΔM) between MALDI peaks and MW of identified proteins, Uniprot protein accession number, and protein names

Figure 1	MALDI MSI	MW (Da)	ΔM (ppm)	Accession No. (Uniprot)	Protein	ROI 1	ROI 2
Α	8569	8565	350	P62982	Ubiquitin-40S ribosomal protein S27a	X	
Α	8569	8565	350	Q63429	Polyubiquitin-C	X	
Α	8569	8565	350	POCG51	Polyubiquitin-B	X	
В	14 041	14 044	285	Q64598	Histone H2A type 1-F-Chain (2-130)	X	
В	14 041	14 045	356	A9UMV8	Histone H2A.J	X	
D	14 132	14 135	283	Q00729	Histone H2B type 1-A-Chain (2-127) b	X	X
D	14132	14 138	495	POCC09	Histone H2A type 2-A b	X	
E	14 192	14 194	211	Q00728	Histone H2A type 4 *	X	
С	14 122	14 121	0	P02688-4	Myelin basic protein isoform 4 ab	X	X
F	14 211	14 211	70	P02688-4	Myelin basic protein isoform 4	X	X
1	17 139	17 136	117	P02688-3	Myelin basic protein isoform 3 ab	X	X
K	18 401	18 398	109	P02688-2	Myelin basic protein isoform 2 ab	X	X
K	18 401	18 401	54	P45592	Cofilin-1-Chain (2-166)	X	
G	15 193	15 197	329	P01946	Hemoglobin subunit alpha-1/2-Chain (2-142)	X	X
Н	15 845	15 847	189	P02091	Hemoglobin subunit beta-1 a	X	X
J	17 737	17 743	395	P10111	Peptidyl-prolyl cis-trans isomerase A-Chain (2-164)	X	
L	21 912	21 914	137	Q99P82	Claudin-11 a	X	
М	22 092	22 088	136	Q99P82	Claudin-11 b	X	X
N	28 217	28 213	106	P68511	14-3-3 protein eta	X	X
N	28 217	28 213	106	P61983	14-3-3 protein gamma <sup>ab</sup>	X	X

aLoss of initial methionine.

<sup>&</sup>lt;sup>b</sup>Acetylation.

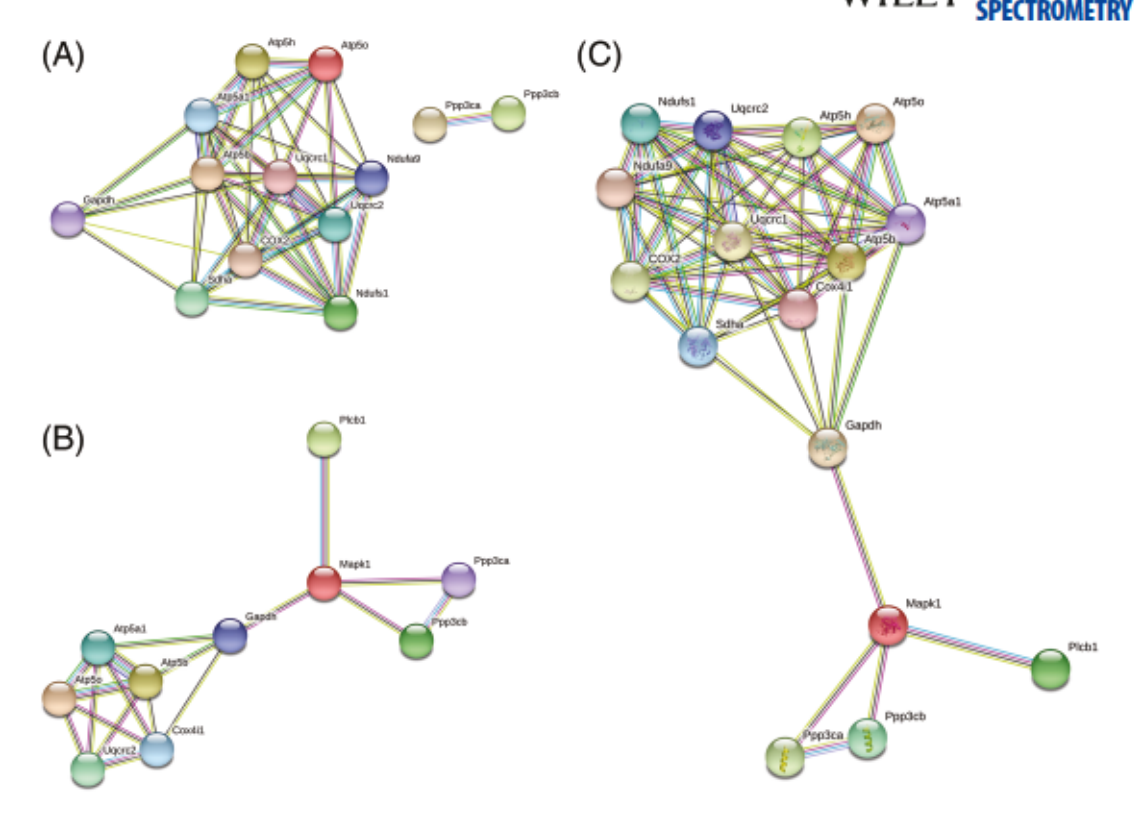


FIGURE 5 KEGG pathway of Alzheimer's disease using protein identified from (A) ROI 1; (B) ROI 2; (C) both ROI 1 and ROI 2

most intense peaks from the MBP family, and the resulting values were normalized using the area of the ablated regions. From UPLC-HDMS<sup>E</sup>, the fraction of all MBP family in ROI 2 was  $66 \pm 5\%$  of that observed in ROI 1.

A pathway analysis of the combined protein lists of the three tissue sections was performed using the database for annotation, visualization, and integrated discovery (DAVID) bioinformatics resource and STRING. MBP is associated with Alzheimer's disease (AD) 70-72; therefore, a pathway analysis using this protein was used to provide a representative illustration of the advantages of localized sampling. Figure 5 shows the network of protein-protein interaction pathways in ROI 1 (A) and ROI 2 (B) both ROI 1 and 2 (C) related to AD (KEGG ID: 05010). The full names of the proteins are listed in Table S3. Six of the proteins were only identified in ROI 1. The protein ndufs1 is deficient in patients with AD,73 and it was identified only in ROI 1 with interactive links to seven other proteins. Three proteins related to AD were identified uniquely in ROI 2. Among them a central role is occupied by Mapk1, which is also implicated in AD,74 and it seems to form a bridge between two interactome areas in ROI 2. An additional pathway analysis was performed using a protein list obtained by merging the proteins identified in ROI 1 and ROI 2; the resulting network plot is displayed in Figure 5C. This combined region plot is similar to what would be expected from an analysis of the entire rat brain section without regard to the expression of proteins in the different parts of the brain.

## 4 | CONCLUSIONS

MALDI imaging directed mid-IR laser ablation was used for protein identification and quantification from rat brain tissue sections. Tissue sections were imaged using MALDI and were used to identify ROI using Gaussian smoothing and contour tracing. The upper quintile of MALDI image from MBP-4 was used as the guide for ROI selection: a 7-mm2 area of the corpus callosum and hippocampus region and a 4-mm<sup>2</sup> square from mid-brain were ablated and transferred. In total, more than 200 to 550 proteins were identified from the different tissue sections in this study. Molecular weights of these proteins and selected post-translationally modified proteins databases were used to identify MALDI MSI peaks. Chain, loss of the initial methionine, and acetylation PTMs together with isoforms were included, resulting in 14 MALDI MSI peaks identified out of 30 peaks. Quantification of the MBP isoform MBP-4 by MALDI imaging revealed that the midbrain region (ROI 2) contained less of that isoform (13 ± 4%) compared with the corpus callosum and hippocampus (ROI 1). The protein isoform MBP-4 could not be quantified by itself using LC-MS/MS because the peptides used to identify that protein are common to all isoforms of MBP, but when the complete set of MPB isoforms was quantified, it was found the midbrain region (ROI 2) contained 66 ± 4% of all isoforms compared with the corpus callosum and hippocampus (ROI 1). This striking difference in quantification results underscores the importance of knowing the protein isoform when comparing MALDI MSI and LC-

MS/MS data. KEGG pathways of the identified proteins were performed to demonstrate localized protein-protein network interactions. MALDI MSI directed laser ablation coupled with LC-MS/MS may be used to further investigate protein-protein network by linking protein interactions to their actual localization in a tissue specimen.

#### **ACKNOWLEGEMENTS**

This work was supported by the National Science Foundation Grant Number CHE-1709526.

#### COMPLIANCE WITH ETHICAL STANDARDS

#### CONFLICT OF INTEREST

The authors declare that they have no conflict of interest.

#### ORCID

Kelin Wang https://orcid.org/0000-0003-4162-3653

Fabrizio Donnarumma https://orcid.org/0000-0003-1397-9919

Michael E. Pettit https://orcid.org/0000-0002-8048-9875

Carson W. Szot https://orcid.org/0000-0001-5752-6220

Touradj Solouki https://orcid.org/0000-0002-4209-9200

Kermit K. Murray https://orcid.org/0000-0002-4976-2263

#### REFERENCES

- Gessel MM, Norris JL, Caprioli RM. MALDI imaging mass spectrometry: spatial molecular analysis to enable a new age of discovery. J. Proteomics. 2014;107:71-82.
- Schwambom K, Kriegsmann M, Weichert W. MALDI imaging mass spectrometry—from bench to bedside. Biochim. Biophys. Acta, Proteins Proteomics. 2017;1865(7):776-783.
- Baker TC, Han J, Borchers CH. Recent advancements in matrixassisted laser desorption/ionization mass spectrometry imaging. Curr. Opin. Biotechnol. 2017;43:62-69.
- Kriegsmann J, Kriegsmann M, Casadonte R. MALDI TOF imaging mass spectrometry in clinical pathology: a valuable tool for cancer diagnostics. Int. J. Oncol. 2015;46(3):893-906.
- Chatterji B, Pich A. MALDI imaging mass spectrometry and analysis of endogenous peptides. Expert Rev. Proteomics. 2013;10(4):381-388.
- Sparvero LJ, Amoscato AA, Dixon CE, et al. Mapping of phospholipids by MALDI imaging (MALDI-MSI): realities and expectations. Chem. Phys. Lipids. 2012;165(5):545-562.
- Aichler M, Walch A. MALDI imaging mass spectrometry: current frontiers and perspectives in pathology research and practice. Lab. Invest. 2015;95(4):422-431.
- Quanico J, Franck J, Wisztorski M, Salzet M, Foumier I. Progress and potential of imaging mass spectrometry applied to biomarker discovery. Progress and Potential of Imaging Mass Spectrometry Applied to Biomarker Discovery. In: Kobeissy F, Stevens S Jr. eds. Neuroproteomics. Methods in Molecular Biology, vol 1598. New York, NY: Humana Press; 2017.
- Ucal Y, Durer ZA, Atak H, et al. Clinical applications of MALDI imaging technologies in cancer and neurodegenerative diseases. Biochim. Biophys. Acta, Proteins Proteomics. 2017;1865(7):795-816.

- Lodén H, Shariatgorji M, Nilsson A, Andrén PE. An introduction to MS imaging in drug discovery and development. Bioanalysis. 2015; 7(20):2621-2627.
- van de Ven SM, Bemis KD, Lau K, et al. Protein biomarkers on tissue as imaged via MALDI mass spectrometry: a systematic approach to study the limits of detection. *Proteomics*. 2016;16(11-12):1660-1669.
- Stastna M, Van Eyk JE. Analysis of protein isoforms: can we do it better? Proteomics. 2012;12(19–20):2937-2948.
- Kim M-S, Pinto SM, Getnet D, et al. A draft map of the human proteome. Nature. 2014;509:575-581.
- Vaysse P-M, Heeren RM, Porta T, Balluff B. Mass spectrometry imaging for clinical research—latest developments, applications, and current limitations. Analyst. 2017;142(15):2690-2712.
- McDonnell L, Angel P, Lou S, Drake R. Mass spectrometry imaging in cancer research: future perspectives. Adv. Cancer Res. 2017;283-290.
- Laskin J, Lanekoff I. Ambient mass spectrometry imaging using direct liquid extraction techniques. Anal. Chem. 2015;88(1):52-73.
- Quanico J, Franck J, Dauly C, et al. Development of liquid microjunction extraction strategy for improving protein identification from tissue sections. J. Proteomics. 2013;79:200-218.
- Quanico J, Franck J, Cardon T, et al. NanoLC-MS coupling of liquid microjunction microextraction for on-tissue proteomic analysis. Biochim. Biophys. Acta. Proteins Proteomics. 2017;1865(7):891-900.
- Schey KL, Anderson DM, Rose KL. Spatially-directed protein identification from tissue sections by top-down LC-MS/MS with electron transfer dissociation. Anal. Chem. 2013;85(14):6767-6774.
- Théron L, Centeno D, Coudy-Gandilhon C, et al. A proof of concept to bridge the gap between mass spectrometry imaging, protein identification and relative quantitation: MSI~ LC-MS/MS-LF. Proteomes. 2016;4(4):32.
- Delcourt V, Franck J, Leblanc E, et al. Combined mass spectrometry imaging and top-down microproteomics reveals evidence of a hidden proteome in ovarian cancer. Ebiomedicine. 2017;21:55-64.
- Le Rhun E, Duhamel M, Wisztorski M, et al. Evaluation of nonsupervised MALDI mass spectrometry imaging combined with microproteomics for glioma grade III classification. Biochim. Biophys. Acta, Proteins Proteomics. 2017;1865(7):875-890.
- Kristiansen G. Manual Microdissection. Methods Mol. Biol. 2010;576:31-38.
- Hunt JL, Finkelstein SD. Microdissection techniques for molecular testing in surgical pathology. Arch. Pathol. Lab. Med. 2004;128(12):1372-1378.
- Franck J, Quanico J, Wisztorski M, Day R, Salzet M, Fournier L Quantification-based mass spectrometry imaging of proteins by parafilm assisted microdissection. Anal. Chem. 2013;85(17):8127-8134.
- Quanico J, Franck J, Wisztorski M, Salzet M, Fournier I. Combined MALDI mass spectrometry imaging and parafilm-assisted microdissection-based LC-MS/MS workflows in the study of the brain. Methods Mol. Biol. 2017;1598:269-283.
- Quanico J, Franck J, Gimeno J, et al. Parafilm-assisted microdissection: a sampling method for mass spectrometry-based identification of differentially expressed prostate cancer protein biomarkers. Chem. Commun. 2015;51(22):4564-4567.
- Datta S, Malhotra L, Dickerson R, Chaffee S, Sen CK, Roy S. Laser capture microdissection: big data from small samples. Histol. Histopathol. 2015;30(11):1255-1269.
- Emmert-Buck MR, Bonner RF, Smith PD, et al. Laser capture microdissection. Science. 1996;274(5289):998-1001.

- Mahalingam M. Laser Capture Microdissection: Insights into Methods and Applications. In: Murray G eds. Laser Capture Microdissection. Methods in Molecular Biology, vol 1723. New York, NY: Humana Press; 2018.
- Vandewoestyne M, Goossens K, Burvenich C, Van Soom A, Peelman L, Deforce D. Laser capture microdissection: should an ultraviolet or infrared laser be used? Anal. Biochem. 2013;439(2):88-98.
- Tayade C, Edwards AK, Bidarimath M. Laser Capture Microdissection.
   In: Croy BA, Yamada AT, deMayo FJ, Adamson SL eds. The Guide to Investigation of Mouse Pregnancy. London, UK: Academic Press (Elsevier): 2014:567-575.
- Tikka S, Monogioudi E, Gotsopoulos A, et al. Proteomic profiling in the brain of CLN1 disease model reveals affected functional modules. Neuromolecular Med. 2016;18(1):109-133.
- Marques JV, Dalisay DS, Yang H, Lee C, Davin LB, Lewis NG. A multiomics strategy resolves the elusive nature of alkaloids in Podophyllum species. Mol. Biosyst. 2014;10(11):2838-2849.
- Dilillo M, Ait-Belkacem R, Esteve C, et al. Ultra-high mass resolution MALDI imaging mass spectrometry of proteins and metabolites in a mouse model of glioblastoma. Sci. Rep. 2017;7(1):603-613.
- Djidja M-C, Chang J, Hadjiprocopis A, et al. Identification of hypoxiaregulated proteins using MALDI-mass spectrometry imaging combined with quantitative proteomics. J. Proteome Res. 2014; 13(5):2297-2313.
- Mittal P, Klingler-Hoffmann M, Arentz G, et al. Lymph node metastasis of primary endometrial cancers: associated proteins revealed by MALDI imaging. Proteomics. 2016;16(11-12):1793-1801.
- Alberts D, Pottier C, Smargiasso N, et al. MALDI imaging-guided microproteomic analyses of heterogeneous breast tumors—a pilot study. Prot. Clin. Appl. 2018; 12, 1700062.
- Lorenz M, Ovchinnikova OS, Van Berkel GJ. Fully automated laser ablation liquid capture surface analysis using nanoelectrospray ionization mass spectrometry. Rapid Commun. Mass Spectrom. 2014; 28(11):1312-1320.
- Cahill JF, Kertesz V, Van Berkel GJ. Characterization and application of a hybrid optical microscopy/laser ablation liquid vortex capture/electrospray ionization system for mass spectrometry imaging with sub-micrometer spatial resolution. Anal. Chem. 2015;87(21): 11113-11121.
- Ovchinnikova OS, Kertesz V, Van Berkel GJ. Combining laser ablation/liquid phase collection surface sampling and highperformance liquid chromatography-electrospray ionization-mass spectrometry. Anal. Chem. 2011;83(6):1874-1878.
- Park S-G, Murray KK. Infrared laser ablation sample transfer for MALDI imaging. Anal. Chem. 2012;84(7):3240-3245.
- Donnarumma F, Cao F, Murray KK. Laser ablation with vacuum capture for MALDI mass spectrometry of tissue. J. Am. Soc. Mass Spectrom. 2016;27(1):108-116.
- O'Brien JT, Williams ER, Holman H-YN. Ambient infrared laser ablation mass spectrometry (AIRLAB-MS) of live plant tissue with plume capture by continuous flow solvent probe. Anal. Chem. 2015;87(5): 2631-2638.
- Ren L, Robertson W, Reimer R, et al. Towards instantaneous cellular level bio diagnosis: laser extraction and imaging of biological entities with conserved integrity and activity. Nanotechnology. 2015; 26(28):284001.
- Park S-G, Murray KK. Laser Ablation Sample Transfer for Mass Spectrometry Imaging. In: He L, eds. Mass Spectrometry Imaging of Small Molecules. Methods in Molecular Biology (Methods and Protocols), vol 1203. New York, NY: Humana Press; 2015.

- Park SG, Murray KK. Ambient laser ablation sampling for capillary electrophoresis mass spectrometry. Rapid Communications in Mass Spectrometry. 2013;27(15):1673-1680.
- Park SG, Murray KK. Infrared laser ablation sample transfer for on-line liquid chromatography electrospray ionization mass spectrometry. J. Mass Spectrom. 2012;47(10):1322-1326.
- Park S-G, Murray KK. Infrared laser ablation sample transfer for MALDI and electrospray. J. Am. Soc. Mass Spectrom. 2011; 22(8):1352-1362.
- Donnarumma F, Murray KK. Laser ablation sample transfer for localized LC-MS/MS proteomic analysis of tissue. J. Mass Spectrom. 2016;51(4):261-268.
- Caldwell KL, Ryan McGarity D, Murray KK. Matrix-assisted laser desorption/ionization with a tunable mid-infrared optical parametric oscillator. J. Mass Spectrom. 1997;32(12):1374-1377.
- Little MW, Laboy J, Murray KK. Wavelength dependence of soft infrared laser desorption and ionization. J. Phys. Chem. C. 2007; 111(3):1412-1416.
- Wang K, Donnarumma F, Baldone MD, Murray KK. Infrared laser ablation and capture of enzymes with conserved activity. Anal. Chim. Acta. 2018;1027;41-46.
- Wang K, Donnarumma F, Herke SW, Herke PF, Murray KK. Infrared laser ablation sample transfer of tissue DNA for genomic analysis. Analytical Bioanal. Chem. 2017;409(17):4119-4126.
- Wang K, Donnarumma F, Herke SW, Dong C, Herke PF, Murray KK. RNA sampling from tissue sections using infrared laser ablation. Anal. Chim. Acta. 2019;1063:91-98.
- Banstola B, Grodner ET, Cao F, Donnarumma F, Murray KK. Systematic assessment of surfactants for matrix-assisted laser desorption/ionization mass spectrometry imaging. Anal. Chim. Acta. 2017;963:76-82.
- Chaurand P, Norris JL, Cornett DS, Mobley JA, Caprioli RM. New developments in profiling and imaging of proteins from tissue sections by MALDI mass spectrometry. J. Proteome Res. 2006; 5(11):2889-2900.
- Hughes CS, Foehr S, Garfield DA, Furlong EE, Steinmetz LM, Krijgsveld J. Ultrasensitive proteome analysis using paramagnetic bead technology. Mol. Syst. Biol. 2014;10:757.
- Huang DW, Sherman BT, Lempicki RA. Systematic and integrative analysis of large gene lists using DAVID bioinformatics resources. Nat. Protoc. 2008;4:44-57.
- Huang DW, Sherman BT, Lempicki RA. Bioinformatics enrichment tools: paths toward the comprehensive functional analysis of large gene lists. Nucleic Acids Res. 2008;37(1):1-13.
- Szklarczyk D, Franceschini A, Wyder S, et al. STRING v10: proteinprotein interaction networks, integrated over the tree of life. Nucleic Acids Res. 2014;43:D447-D452.
- Khayer N, Zamanian-Azodi M, Mansouri V, et al. Oral squamous cell cancer protein-protein interaction network interpretation in comparison to esophageal adenocarcinoma. Gastroenterol. Hepatol. Bed Bench. 2017; 10(2):118-124.
- Von Mering C, Jensen LJ, Snel B, et al. STRING: known and predicted protein-protein associations, integrated and transferred across organisms. Nucleic Acids Res. 2005;33:D433-D437.
- 64. Zavalin A, Yang J, Hayden K, Vestal M, Caprioli RM. Tissue protein imaging at 1 μm laser spot diameter for high spatial resolution and high imaging speed using transmission geometry MALDI TOF MS. Anal. Bioanal. Chem. 2015;407(8):2337-2342.

- Lin L-E, Su P-R, Wu H-Y, Hsu C-C. A simple sonication improves protein signal in matrix-assisted laser desorption ionization imaging. J. Am. Soc. Mass Spectrom. 2018;29(4):796-799.
- Khazipov R, Zaynutdinova D, Ogievetsky E, et al. Atlas of the postnatal rat brain in stereotaxic coordinates. Front. Neuroanat. 2015;9:161.
- Pettit ME, Donnarumma F, Murray KK, Solouki T. Infrared laser ablation sampling coupled with data independent high resolution UPLC-IM-MS/MS for tissue analysis. Anal. Chim. Acta. 2018;1034: 102-109.
- Akiyama K, Ichinose S, Omori A, Sakurai Y, Asou H. Study of expression of myelin basic proteins (MBPs) in developing rat brain using a novel antibody reacting with four major isoforms of MBP. J. Neurosci. Res. 2002;68(1):19-28.
- Wisztorski M, Desmons A, Quanico J, et al. Spatially-resolved protein surface microsampling from tissue sections using liquid extraction surface analysis. Proteomics. 2016;16(11–12):1622-1632.
- Zhan X, Jickling GC, Ander BP, et al. Myelin basic protein associates with AβPP, Aβ 1-42, and amyloid plaques in cortex of Alzheimer's disease brain. J. Alzheimers Dis. 2015;44(4):1213-1229.
- Liao M-C, Ahmed M, Smith SO, Van Nostrand WE. Degradation of amyloid β protein by purified myelin basic protein. J. Biol. Chem. 2009;284(42):28917-28925.

- Ou-Yang M-H, Van Nostrand WE. The absence of myelin basic protein promotes neuroinflammation and reduces amyloid β-protein accumulation in Tg-5xFAD mice. J. Neuroinflammation. 2013;10:901-912.
- Kim SH, Vlkolinsky R, Cairns N, Fountoulakis M, Lubec G. The reduction of NADH: ubiquinone oxidoreductase 24-and 75-kDa subunits in brains of patients with Down syndrome and Alzheimer's disease. Life Sci. 2001;68(24):2741-2750.
- Munoz L, Ammit AJ. Targeting p38 MAPK pathway for the treatment of Alzheimer's disease. Neuropharmacology. 2010;58(3):561-568.

## SUPPORTING INFORMATION

Additional supporting information may be found online in the Supporting Information section at the end of the article.

How to cite this article: Wang K, Donnarumma F, Pettit ME, Szot CW, Solouki T, Murray KK. MALDI imaging directed laser ablation tissue microsampling for data independent acquisition proteomics. J Mass Spectrom. 2020;55:e4475. <a href="https://doi.org/10.1002/jms.4475">https://doi.org/10.1002/jms.4475</a>